Available online at www.sciencedirect.com
SCIENCE DIRECT
Journal of Magnetic Resonance 179 (2006) 206–216
JMR Journal of Magnetic Resonance
www.elsevier.com/locate/jmr

Selective refocusing pulses in magic-angle spinning NMR: Characterization and applications to multi-dimensional protein spectroscopy

Ying Li, Benjamin J. Wylie, Chad M. Rienstra *

Department of Chemistry and Center for Biophysics and Computational Biology, University of Illinois at Urbana-Champaign, 600 South Mathews Avenue, Urbana, IL 61801, USA

Received 1 September 2005; revised 22 November 2005
Available online 10 January 2006

Abstract

Band-selective pulses are frequently used in multi-dimensional NMR in solution, but have been used relatively less often in solid-state NMR applications because of the complications imposed by magic-angle spinning. In this work, we examine the frequency profiles and the refocusing efficiency of several commonly employed selective general rotation π pulses through experiments and numerical simulations. We demonstrate that highly efficient refocusing of transverse magnetization can be achieved, with experiments that agree well with numerical simulations. We also show that the rotational echo is shifted by a half rotor period if a selective pulse is applied over an integer number of rotor periods. Appropriately synchronizing indirect evolution periods with selective pulses ensures proper phasing of cross peaks in 2D spectra. The improved performance of selective pulses in multi-dimensional protein spectroscopy is demonstrated on the 56-residue β1 immunoglobulin binding domain of protein G (GB1).

Keywords: Solid-state NMR spectroscopy; Selective pulses; Rotational echo; Scalar coupling; Protein

1. Introduction

Band-selective pulses are routinely used in solution NMR to achieve spectral simplification, resolution enhancement and water suppression [1,2]. More recently, it has been demonstrated that selective pulses can also benefit various types of solid-state NMR (SSNMR) experiments, particularly on uniformly or extensively labeled peptides and proteins. Under fast magic-angle spinning (MAS), homonuclear scalar (*J*) couplings contribute a large portion of the line width for peptide and protein samples prepared with narrow inhomogeneous line widths [3–8]. *J*-decoupling in the indirect dimension(s) has been demonstrated to be an efficient way to improve spectral resolution on both solid peptide [6] and protein [3,5,7,8] samples. Spectral resolution can also be improved through spin state selection experiments [9,10], in which a single component of the multiplet is selected. Both types of experiments rely on band-selective pulses. When anisotropic interactions such as the dipolar coupling and chemical shift anisotropy (CSA) are measured, the presence of homonuclear *J*-coupling effects is often undesirable. By using selective pulses to refocus *J* coupling evolution, the precision of weak dipolar coupling [11] and CSA measurements [12,13] is improved. Selective pulses have also been used in the frequency selective REDOR experiment to selectively recouple ^{15}N and ^{13}C nuclei within desired chemical shift ranges [14–16].

Thus far, most applications of selective pulses in rotating solids have relied upon relatively simple DANTE [5,8,12] or Gaussian pulses [6,9,13,15], with one exception of r-SNOB pulses used for band-selective carbonyl-decoupling [7]. The relative simplicity of the DANTE and Gaussian pulses makes their implementation relatively straightforward, but comes with the compromise of far

* Corresponding author. Fax: +1 217 244 3186.
E-mail address: rienstra@scs.uiuc.edu (C.M. Rienstra).

1090-7807/$ - see front matter © 2005 Elsevier Inc. All rights reserved.
doi:10.1016/j.jmr.2005.12.003

from uniform excitation profiles and poor overall efficiency. The utilization of computer-optimized selective pulses originally developed for solution NMR may alleviate some of these problems and lead to generally improved performance. The BURP, SNOB and Gaussian cascade pulse families are several very successful examples of computer-optimized pulses that are widely used in solution NMR [17,18]. BURP pulses give excitation of uniform intensity and pure phase [19]. r-SNOB pulses enable time efficient excitation with an improved excitation profile over other RF pulses of similar duration [20]. Gaussian cascade pulses [21,22] give significantly improved frequency profiles over Gaussian pulses without sacrificing the easy implementation of Gaussian pulses. In MAS experiments, it is likely that the performance of these pulses will depend on specific experimental conditions, due to the complications brought about by large anisotropic interactions modulated by MAS. In this work, we characterize the time symmetric RE-BURP and r-SNOB pulses and time asymmetric Q3 pulse as refocusing pulses by performing experiments and numerical simulations under the conditions commonly used for protein MAS NMR spectroscopy.

Although several studies [3,5–8] have already demonstrated the success of applying selective pulses to achieve *J*-decoupling in the indirect dimension of multi-dimensional chemical shift correlation experiments, the problem of rotor-synchronizing selective pulses with the indirect evolution period was not specifically addressed. In this work, we address the general problem of rotor synchronization of selective pulses in the context of multi-dimensional experiments. Our results show that an undesirable line shape can result from the incorrect rotor synchronization conditions and an efficient approach to solve this problem is to use selective pulses with pulse width of an integer plus half rotor periods. To evaluate the overall performance of computer-optimized selective pulses in protein spectroscopy, we have performed 2D ^{13}C–^{13}C chemical shift correlation experiments with *J*-decoupling in the ω_1 dimension on a protein β1 immunoglobulin binding domain of protein G (GB1). Our results show that highly efficient refocusing can be achieved and the correct rotor synchronization conditions are essential for optimal spectral sensitivity and resolution.

2. Experimental

N-Acetyl-Valine (NAV) was prepared by synthesis from ^{13}C, ^{15}N-Val and [^{13}C]acetic anhydride (Cambridge Isotopes Laboratory, Andover, MA), and crystallized from methanol [23]. Uniformly ^{13}C,^{15}N-labeled GB1 was prepared and packed into a 3.2 mm thin wall rotor according to Franks et al. [24].

SSNMR experiments were carried out on a 500 MHz Varian (Palo Alto, California) InfinityPlus spectrometer equipped with a Balun ^{1}H–^{13}C–^{15}N 3.2 mm MAS probe. The spinning frequency was set to be 11.111 kHz for all experiments on NAV. Typical π/2 pulse widths were 2.2 μs for ^{1}H, 3 μs for ^{13}C, and 5 μs for ^{15}N. The TPPM ^{1}H decoupling [25] field strength of 75 kHz was used during acquisition. For all selective pulses, the shape functions were digitized with 256 ordinates. Gaussian pulses were truncated at 5% of the maximal amplitude and Sinc pulses were truncated at 3π. A linear amplifier and actively biased transmit-receive switching circuitry are required to ensure the accurate output of these pulse shapes, which have a maximum field strength of only a few kHz, corresponding to peak amplifier powers of less than 1 W. In addition, the feature of the InfinityPlus that enables a coarse amplitude adjustment was utilized, so that the overall pulse shape was scaled by ~12 dB relative to the full amplifier output. The selective pulses were then defined by modulation of the intermediate frequency amplitude with a dynamic range of 4096 points. A short delay (during the chemical shift evolution period) of 3 μs was allocated before and after the selective pulses to allow the change in coarse amplitude scaling factor to take place. The total 6 μs was subtracted from the pulse width of the selective pulses to ensure the proper rotor synchronization of subsequent pulses.

The 1D selective spin-echo pulse sequence contains a ^{1}H to ^{13}C cross-polarization element to create transverse magnetization followed immediately by either a selective π pulse or a pair of selective and non-selective π pulses and an acquisition period with TPPM ^{1}H decoupling (Figs. 1A and B). In general, the TPPM settings will be different during the selective pulse and free evolution periods. Spin pinging [26] phase cycling is implemented to eliminate dispersion components of the signals and obtain pure absorption spectra. The 1D spin-echo pulse sequence with the Hahn echo generated by a hard π pulse contains a delay period τ before and after the hard π pulse. Fig. 1C shows the pulse sequence for 2D ^{13}C–^{13}C chemical shift correlation experiments with *J*-decoupling in the indirect dimension. Resonances within the selected bandwidth are frequency-encoded during the t_1 evolution period and then subjected to longitudinal dipolar assisted rotational resonance (DARR) mixing [27] and detection. A pair of selective and non-selective π pulses is placed in the middle of the t_1 period to refocus the *J*-coupling. *Z*-filters are applied before and after the mixing period. The t_1 increment is set to be two rotor periods to avoid the destructive interference of non-selective π pulse with the rotational echo.

Simulations of frequency profiles and signal intensity were carried out on a single spin-1/2 system using SIMPSON [28]. The experimental CSA tensor values of NAV C′ and Cα resonances reported by Chan and Tycko [29] were used, which are $\delta = 85.4$ ppm, $\eta = 0.488$ for C′ and $\delta = 26.0$ ppm, $\eta = 0.571$ for Cα. The powder average was calculated through 20 γ angles and 168 α/β angles according to the REPULSION averaging scheme [30].

3. Results and discussion

An ideal selective pulse should give uniform excitation in terms of both intensity and phase while minimizing

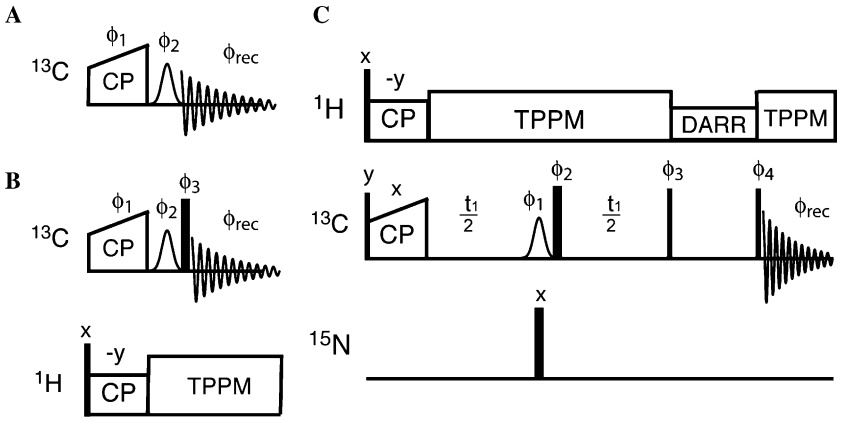

Fig. 1. (A) Pulse sequence diagram of 1D selective spin-echo experiments. The phase cycle is $\phi_1 = 2(x,-x)$ $\phi_2 = (x,y,-x,-y)$ $\phi_{rec} = 2(x,-x)$. (B) Pulse sequence diagram of 1D spin echo experiments with the combination of selective and hard π pulses to achieve an effective 2π rotation. Phase cycle is $\phi_1 = 8(x,-x)$ $\phi_2 = (x,x,y,\ y,x,x,y,y,-x,-y,-x,-y,-x,-y,-x,-y)$ $\phi_3 = 2(x,y,\ x,y,-x,-y,-y,-y)$ $\phi_4 = (x,x,y,y,-x,-x,-y,-y)$ $\phi_{rec} = 4(x,-x,-x,x)$. (C) Pulse sequence diagram of 2D ^{13}C–^{13}C chemical shift correlation experiment with *J*-decoupling in the ω_1 dimension. A r-SNOB pulse is applied in the center of the t_1 period. Phase cycle is $\phi_1 = (x,-x,y,-y,-x,x,-y,y)$ $\phi_2 = (y,-y,-y,y,-y,y,y,-y)$ $\phi_3 = (y,-y,-y,y,-y,y,y,-y)$ $\phi_4 = (x,x,y,y,-x,-x,-y,-y)$ $\phi_{rec} = 2(x,-x,y,-y)$. The quadrature detection in t_1 is achieved by using TPPI, incrementing ϕ_3.

magnetization loss. In practical implementation, there are trade-offs among these features. Pulses with a superior frequency profile tend to have a larger bandwidth-duration product [31] and cause more magnetization loss due to relaxation effects. Consideration of relaxation effects is especially critical in SSNMR experiments, so the choice of selective pulse must consider the overall duration, as well as experimental conditions (B_0 field, spinning frequency, and the magnitude of anisotropic interactions). To evaluate these factors with experimental conditions relevant to peptides and proteins, we characterized r-SNOB, RE-BURP, Gaussian, Q3, and Sinc pulses with the model peptide NAV. The issue of rotor synchronization was addressed to ensure the proper implementation of selective pulses in the context of multi-dimensional experiments.

3.1. The refocusing profile

To assess the feasibility of using computer-optimized selective pulses under MAS, the refocusing profiles of r-SNOB, RE-BURP, Q3, Gaussian, and Sinc pulses were measured with 11.111 kHz MAS frequency for the C′ and Cα resonances of NAV. This MAS frequency avoids both $n = 1$ and $n = 2$ rotational resonance [32] conditions. The selective pulses were timed to span an even number of rotor periods; specific synchronization conditions in the context of 2D experiments will be addressed in greater detail below. In the initial experiments, the duration of each selective pulse was adjusted to give a similar bandwidth of about 15 ppm. This bandwidth is useful, for example, to perform selective refocusing of the C′ region of a typical protein spectrum. We found analogous behavior for slightly larger bandwidths of ~30 ppm, as required for selective Cα refocusing.

Fig. 2 shows the experimental refocusing profiles of different selective pulses (r-SNOB, RE-BURP, Q3, Gaussian, and Sinc) applied to both C′ and Cα resonances of NAV.

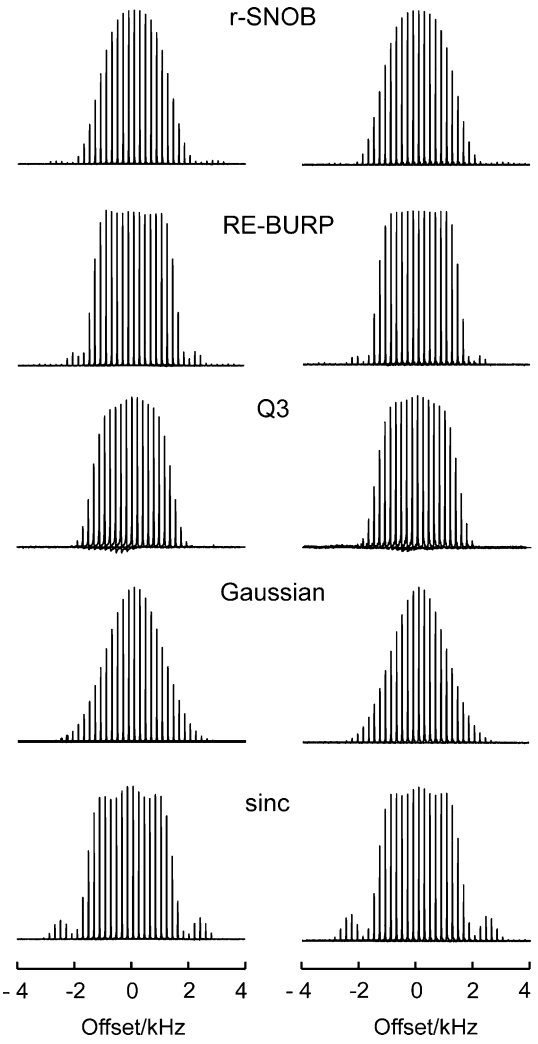

Fig. 2. The experimental refocusing profiles of 900 μs r-SNOB, 1800 μs RE-BURP, 1440 μs Q3, 540 μs Gaussian, and 1440 μs Sinc pulses. The C′ (left column) and Cα (right column) transverse magnetizations of NAV were inverted by the selective pulses. The rotor period is 90 μs. Frequency offset was incremented by 0.2 kHz at each step.

Clearly under the current experimental conditions, the RE-BURP pulse gives the desirable rectangular, or "top hat" response and signals drop off very rapidly (within a ~0.6 kHz frequency range) at the edge. The r-SNOB pulse also gives improved refocusing profiles relative to Gaussian pulses, though the response within the bandwidth is not perfectly uniform due to the sacrifice of uniform response to time efficiency in the original design [20]. In general, no significant deviation of refocusing profiles from target profiles was observed, once the instrumental measures as described above were implemented. For the Q3 pulse, slight phase distortions were observed for both C′ and Cα resonances, apparently due to the fact that Q3 pulse is asymmetric and the flip angle misset cannot be completely compensated.

Compared to Gaussian pulses, the r-SNOB and RE-BURP pulses are more sensitive to flip angle misset. Fig. 3 shows the refocusing profile as a function of flip angle misset for these pulses. Factors that contribute to the flip angle misset include B_1 inhomogeneity, imperfect calibration of selective pulses and CSA. Previous theoretical analysis has been performed to describe the effects of CSA on selective pulses [5,33,34], leading to the conclusion that crystallites experience orientation-dependent RF field scaling factors. Therefore, misset of the flip angle is inevitable for most crystallites. This effect can be minimized by experimentally optimizing the amplitude of selective pulses specific to each experiment. In Fig. 2, the imperfect refocusing profile of RE-BURP on the C′ resonance, especially in transition and suppression regions, is due to this effect.

To evaluate the CSA effects at different B_0 fields, we carried out numerical simulations on a single spin-1/2 system using reported experimental CSA values of NAV C′ resonance. The simulations were performed with parameters corresponding to both 500 MHz and 900 MHz ^{1}H frequencies under the same spinning frequency of 11.111 kHz. As shown in Fig. 4, the frequency profile of RE-BURP at 500 MHz reproduces the features seen in the experimental data. At 900 MHz, the deviation from the target profile is exacerbated in the transition and suppression regions but the responses within the bandwidth are still uniform. The refocusing profiles of r-SNOB pulses are less sensitive to CSA and almost identical at 500 and 900 MHz. For both RE-BURP and r-SNOB pulses, 100% refocusing cannot be achieved even for on-resonance spins when the spinning rate is relatively low compared to the absolute CSA tensor magnitude. In all our simulations, relaxation, homonuclear and heteronuclear couplings to other nuclei are not considered. Therefore, the refocusing efficiency for the on-resonance spins will be lower in the actual experiments, which will be discussed in greater detail below. However, under the experimental conditions we used, signal loss

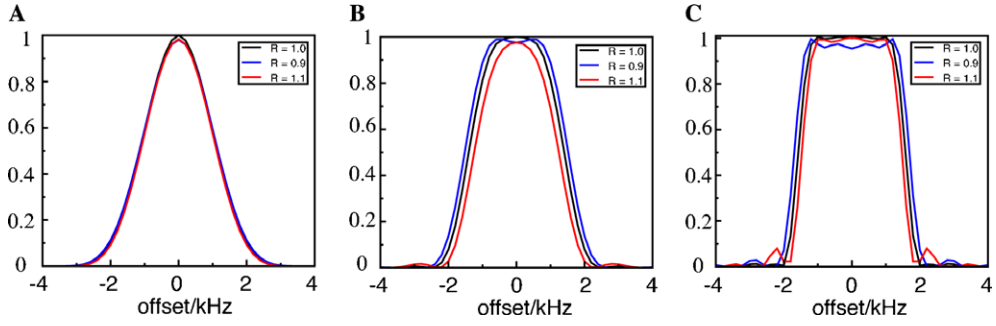

Fig. 3. The simulated refocusing profile of (A) Gaussian, (B) r-SNOB, and (C) RE-BURP as a function of flip angle misset. R is the ratio of actual flip angle to ideal flip angle π. The black line corresponds to $R = 1.0$, the blue line to $R = 0.9$, and the red line to $R = 1.1$. (For interpretation of the references to color in this figure legend, the reader is referred to the web version of this paper.)

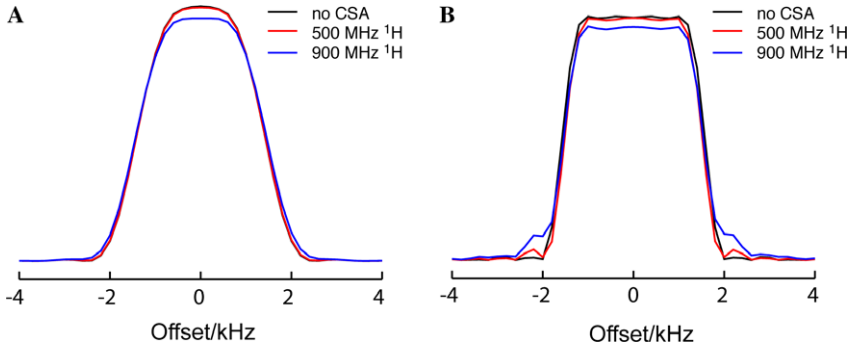

Fig. 4. The simulated refocusing profiles of (A) 900 μs r-SNOB and (B) 1800 μs RE-BURP pulses for a resonance with no CSA (black line), NAV C′ resonance at 500 MHz ^{1}H frequency (red), and the NAV C′ resonance at 900 MHz ^{1}H frequency (blue). The signal intensity was normalized to the original signal created by cross-polarization. The refocusing efficiency for the on-resonance spin with no CSA is 100%. (For interpretation of the references to color in this figure legend, the reader is referred to the web version of this paper.)

caused by CSA is almost negligible. At much lower ratios of spinning frequency to B_0 field, CSA effects could be more dramatic and cause the deformation of frequency profiles which cannot be compensated by even large adjustment of RF power. However, the parameters used in our simulations (900 MHz ^{1}H frequency and 11.111 kHz MAS frequency), in which the intensity of the first order sideband of C′ is ~20% of the centerband, correspond to the lower end of the range of MAS rates typically used for protein spectroscopy. In general, our results therefore apply to the case where greater than 50% of the total intensity is retained in the centerband.

3.2. Heteronuclear ^{1}H decoupling during selective ^{13}C pulses

The magnetization loss during selective pulses is a great concern when experiments are performed on low sensitivity samples. Efficient heteronuclear ^{1}H decoupling during selective pulses is necessary to minimize magnetization loss especially for protonated carbons. We studied the refocusing efficiency as a function of CW decoupling field strength by measuring the echo intensity generated by 900 μs r-SNOB, 1800 μs RE-BURP, and 540 μs Gaussian pulses. The duration of each pulse was chosen to give similar bandwidth. In Figs. 5A and B, the refocusing efficiency is plotted as a function of CW decoupling field strength. The echo intensity is represented as the percentage of the original signal intensity created by cross-polarization. Even for the protonated Cα signal, efficient decoupling (~95% of the signal observed at maximum field) is achieved at modest field strengths (~50 kHz) for both the 900 μs r-SNOB pulse and 540 μs Gaussian pulses. The decoupling field requirement is more demanding for longer pulses such as the 1800 μs RE-BURP, for which the signal intensity continues increasing beyond the field strength of 110 kHz. For the C′ resonance, signals are lowest at the MAS frequency of 11 kHz due to the relatively narrow ^{13}C–^{1}H dipolar assisted rotational resonance (DARR) [27] condition compared to Cα. Because there are no protons directly attached to C′, the required sufficient decoupling fields (to reach 95% of the maximum amplitude) are lower: ~40 kHz for 540 μs Gaussian, ~45 kHz for r-SNOB, and ~57 kHz for 1800 μs RE-BURP.

TPPM is a well-known method to achieve higher ^{1}H decoupling efficiency in rigid solids [25], and is the simplest scheme that yields improvements over CW decoupling within an experimentally relevant range of parameters. However, the interference between the phase modulation of the ^{1}H TPPM decoupling pulses and the amplitude modulation of the selective pulses applied on the ^{13}C channel could compromise its efficiency. We performed 1D spin-echo experiments to determine whether TPPM decoupling could be successfully applied during selective pulses. TPPM conditions (at field strength of ~80 kHz) were optimized separately for each selective pulse. The typical optimal conditions were ~6.0 μs pulse width and 15° phase shift. Figs.

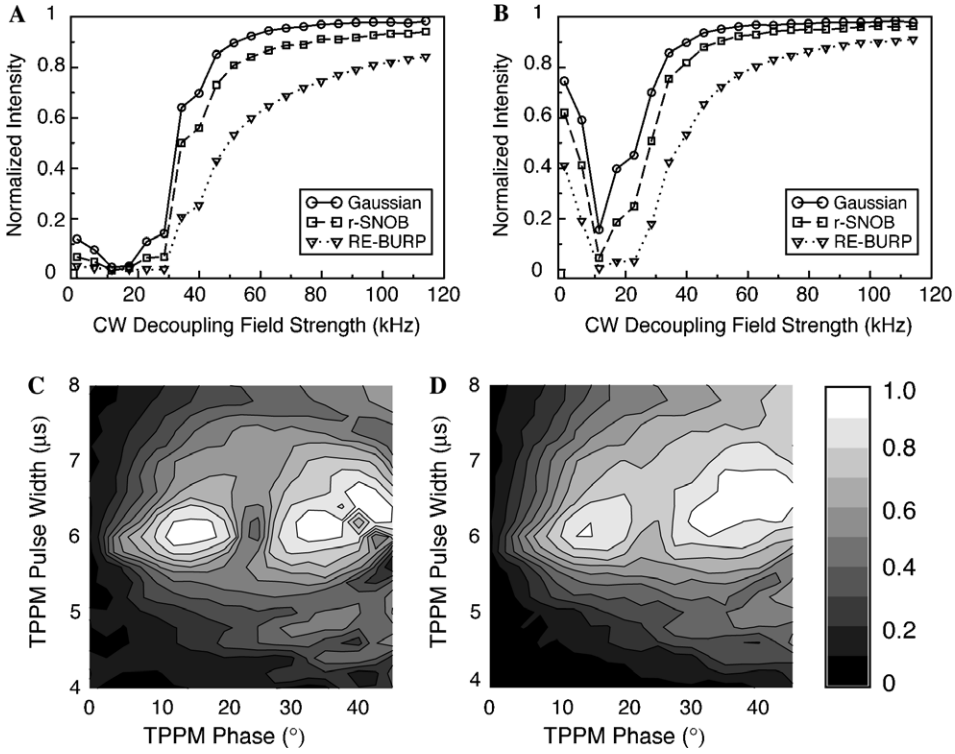

Fig. 5. Normalized signal intensity as a function of CW decoupling field strength during selective pulses on NAV (A) Cα resonance and (B) C′ resonance. The selective pulses applied are 540 μs Gaussian, 900 μs r-SNOB, and 1800 μs RE-BURP pulses. The signal intensity is normalized to the original signal created by cross-polarization. 2D contour plots showing the signal intensity as a function of the pulse width and phase shift of TPPM decoupling during 1800 μs RE-BURP for NAV (C) Cα resonance and (D) C′ resonance.

5C and D show the normalized signal intensity as a function of both pulse width and (total) phase shift of TPPM decoupling during a 1800 μs RE-BURP pulse on Cα and C′. For both resonances, the highest decoupling efficiency was found under a relatively narrow range of conditions though the variation in signal intensity is more significant for Cα than C. At the optimal conditions, TPPM decoupling gives an improvement of 21% for Cα and 10% for C′ over CW decoupling at the same field strength during a 1800 μs RE-BURP pulse. For 900 μs r-SNOB, the improvement is less dramatic and is 4% for Cα and 0.5% for C′. The improvement is less than 1% for a 540 μs Gaussian on both Cα and C′. Therefore, experiments using long selective pulses on protonated carbons will benefit most from TPPM decoupling, and we expect the amplitude of this effect to increase at higher magnetic fields, where phase-modulated decoupling schemes will be critical for optimal implementation of selective pulses. As demonstrated by Duma et al. [9], other more recently developed decoupling schemes such as eDROOPY could also be applied during selective refocusing period to give further improvement under certain experimental conditions.

3.3. Selective refocusing π pulses induce shift of rotational echo

In our 1D experiments with selective pulses, we observed an interesting phenomenon: the phase of the first order sideband is shifted by 180° with respect to the centerband for all pulses of an integer number of rotor periods. A few theoretical studies have been published on selective pulses, including the original work by Caravatti et al. [34] in the 1980s as well as more recent studies [5,33]. All these studies adopted very similar approaches, leading to the conclusion that dispersion components of the sidebands that are off-resonance are completely cancelled out based on the symmetry properties [35]. Since all studies treat the selective pulse as a constant amplitude rectangular pulse for simplification, the conclusion should be generic and not associated with any particular pulse shape. The only prerequisite is that the pulse duration should be an integer number of rotor periods. At lower spinning rates, higher order average Hamiltonian terms need to be considered to accurately predict experimental results. Although it is correctly predicted by theory that the off-resonance sideband family should be absorptive, the experimental observation of the sign and magnitude (in particular zero or non-zero) of the real components of the sidebands has not been adequately explained by theory and likely depends on the specific context (excitation, inversion or refocusing) in which the selective pulses are applied. Cavatti et al. [34] observed that the sidebands vanish when magnetization is excited by a non-synchronized DANTE pulse train. Igumenova and McDermott [5] demonstrated by experiments that the first order sidebands are 180° out of phase with respect to the centerband when transverse magnetization is inverted by a non-synchronized DANTE pulse train on resonance with the centerband. Fig. 6A shows the

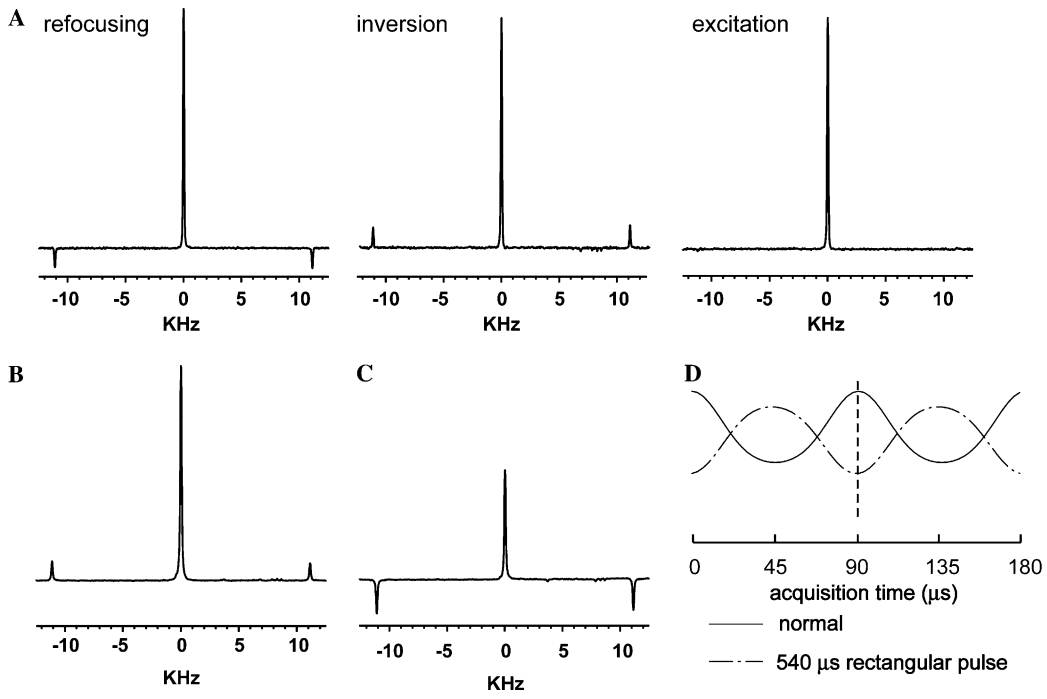

Fig. 6. (A) 1D ^{13}C spectra with transverse magnetization of the C′ resonance refocused by 540 μs rectangular pulse and longitudinal magnetization inverted and excited by 540 μs rectangular pulse. (B) Carbonyl region of 1D ^{13}C spectrum of NAV acquired with the 1D spin-echo sequence, in which the Hahn echo was generated by a hard π pulse. The delay τ before and after the π pulse is 540 μs (6.0 rotor periods). (C) Carbonyl region of 1D ^{13}C spectrum of NAV acquired with the same sequence and parameters as (B) but with the delay $\tau = 585$ μs (6.5 rotor periods). (D) The simulated normal rotational echo and the rotational echo after 540 μs rectangular refocusing pulse on resonance of NAV C′. The rotor period is 90 μs.

results we obtained by using a low amplitude rectangular pulse with duration of an integer number of rotor periods. Here we used a rectangular pulse to ensure our observation is not associated with a particular pulse shape. Our results are consistent with previous studies. In addition, we observed that in the case of an inversion π pulse the sign of the first order sideband remains the same as the centerband. We also note a similarity to the well-known effect of rotor-asynchronous hard π pulses causing a relative change of sign in the centerband and sidebands. Fig. 6B shows a standard rotor-synchronized Hahn echo with a hard π pulse, with an integer number of rotor periods before and after the π pulse. All sidebands are in phase. Fig. 6C shows the effect of improper synchronization, where the hard π pulse is placed in the middle of a rotor period, disrupting the rotor echo. Signal intensity is lost in the centerband, and the first-order sidebands are inverted. This represents, for the C′ region of the spectrum, an effect analogous to our observations with shaped pulses, which invert only the centerband.

To further analyze this phenomenon, we simulated the selective Hahn echo experiments using a single spin-1/2 system. Our simulations agree well with experiments and enable us to examine this phenomenon in the time domain with a simplified spin-1/2 system, to facilitate experimental design. Fig. 6D shows the simulated time domain signal of on-resonance transverse magnetization inverted by a rectangular π pulse with a pulse width of six rotor periods; the rotational echo has been shifted in time by half a rotor period. Although the spins are dephased immediately after the selective pulse, they are largely refocused by sample rotation after half a rotor period and therefore no significant loss in centerband intensity should be expected even when the CSA is relatively large.

Since the phase of a sideband only depends on the pulse width with respect to the rotor period, we performed experiments to understand the phase of a sideband as a function of pulse width. As shown in Fig. 7A, for selective pulses of an integer number of rotor periods, the first order sideband is 180° out of phase with respect to the centerband. The phase of the first order sideband changes continuously with the pulse width and becomes the same as the center band at an integer plus half rotor periods. Simulations were also performed to examine the time domain picture. As shown in Fig. 7B, the effect of shifted rotational echo can be compensated by using selective pulses of an integer plus half

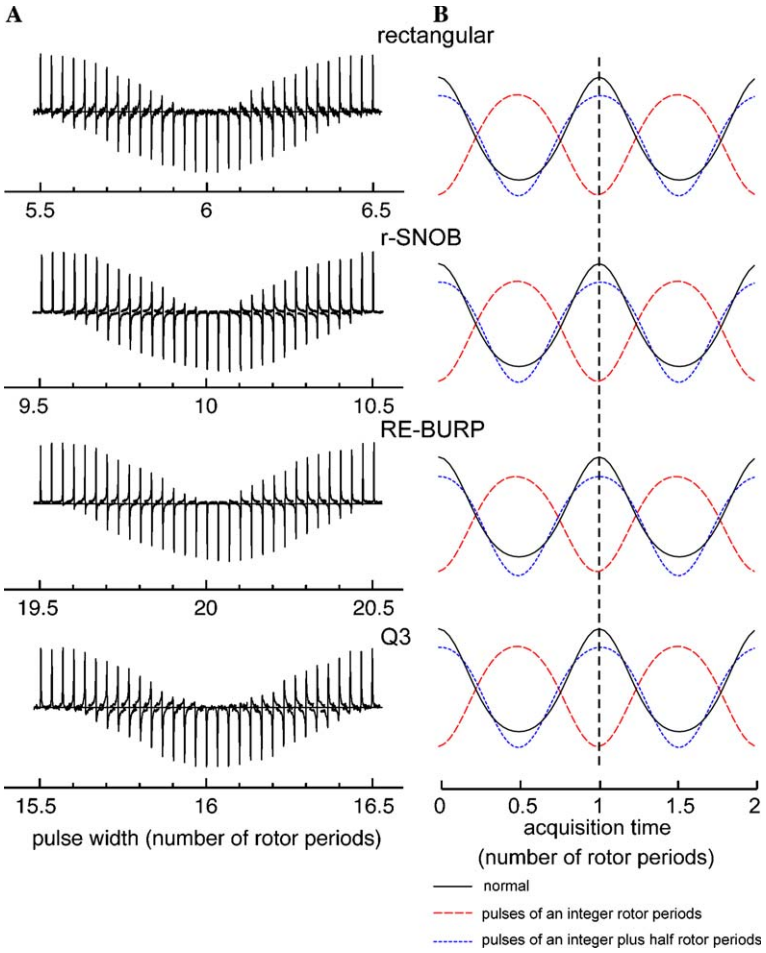

Fig. 7. (A) The dependence of sideband phase on the pulse width of rectangular, r-SNOB, RE-BURP, and Q3 pulses applied to refocus the transverse magnetization. The centerband was phased to be positive. (B) Simulated normal rotational echo and rotational echoes after a selective pulse (rectangular, r-SNOB, RE-BURP or Q3) of either an integer or an integer plus half rotor periods with the exact numbers the same as in (A).

rotor periods. It is also clear from both Figs. 7A and B that different shaped pulses give essentially the same results for both experimental spectra and simulated time domain signals.

3.4. Rotor synchronization of selective pulses

In this section, we discuss the rotor synchronization condition of selective pulses in multi-dimensional *J*-decoupling experiments. We followed previously published *J*-decoupling protocols [5,6], except the pulse width of the selective pulses was varied in our experiments. Specifically, the dwell time of the indirect evolution period was set to be two rotor periods to ensure the same rotor phase for each sampling point. Spin-echo 1D experiments were performed on the C′ resonance of NAV to identify possible rotor synchronization conditions. We chose the C′ resonance due to the fact that it has a large CSA magnitude and therefore any effects that are associated with CSA will be more dramatic and more easily identifiable experimentally. Since it is clear from previous discussion that the rotor-synchronization conditions are not likely to depend on the pulse shape, we used only the r-SNOB pulse as an example for all our experiments in this section. A series of 1D ^{13}C spectra were acquired with transverse magnetization rotated by 2π by a combination of selective and hard π pulses and varied pulse widths of selective pulse (pulse sequence diagram shown in Fig. 1B). The duration of the r-SNOB pulse was varied from 9.5 to 10.5 rotor periods. Fig. 8A shows the centerband intensity as a function of pulse width, which changes continuously with the pulse width; the maximal intensity was found at 9.5 and 10.5 rotor periods. The minimal intensity is only 50% of the maximal and found at 10 rotor periods. The significantly depressed centerband intensity is accounted for by the destructive interference between the shifted rotational echo and the hard π pulse.

Since it is known from the 1D experiments that the time shift of the rotational echo can be compensated for by extending the pulse width by a half rotor period, we explored the rotor synchronization condition in the context of multi-dimensional experiments. We performed 2D ^{13}C–^{13}C correlation experiments with *J*-decoupling in the indirect evolution period. In this sequence, transverse magnetization evolves in the t_1 period and then is subjected to longitudinal mixing. Since the magnetization is rotated to the *z* direction at the end of the t_1 evolution period, all spins must be in phase at this time point. To fulfill this requirement the destructive interference of a hard π pulse with the rotational echo needs to be avoided. There are at least two ways to avoid the undesirable interference. One way is to place the hard π pulse before the selective π pulse with duration of an integer number of rotor periods. However, due to the time shift of the rotational echo by the selective π pulse, the spins will not be completely in phase at the end of t_1 period. The alternative of extending the second half of the t_1 evolution period by half a rotor period to ensure sampling at the rotational echo gives an asymmetric distribution of the t_1 period before and after the π pulses, leading to imperfect refocusing of the *J*-coupling. A second approach, which we have found to be superior, is to use selective pulse of an integer plus half rotor periods. In this case, no matter whether the hard π pulse is placed before or after the selective π pulse, there is no destructive interference and a normal rotational echo is maintained through the second half of t_1 period. This second solution enables standard chemical shift evolution and *J*-decoupling strategies to be utilized, achieving pure-phase spectra in the indirect dimension.

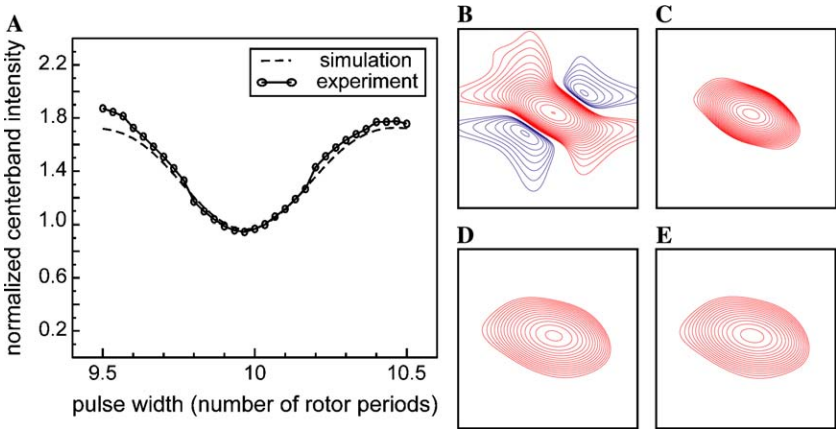

Fig. 8. (A) The experimental and simulated centerband intensity as a function of the pulse width of an r-SNOB pulse when both selective and non-selective π pulses are applied to generate an echo. The peak intensity generated by an r-SNOB pulse of 10 rotor periods is normalized to 1 for both simulated and experimental spectra. The pulse width of r-SNOB pulses is varied from 9.5 to 10.5 rotor periods with an increment of 1/30 rotor period. (B–E) 2D ^{13}C–^{13}C spectra of NAV with homonuclear *J*-decoupling in the ω_1 dimension. C′–C′ diagonal peaks in 2D spectra acquired with (B) 900 μs r-SNOB and (C) 945 μs r-SNOB on C′. Cα–Cα diagonal peaks in 2D spectra acquired with (D) 900 μs r-SNOB and (E) 945 μs r-SNOB on Cα. The rotor period is 90 μs. The acquisition parameters for 2D experiments are 2 ms ^{1}H–^{13}C CP contact time, 75 kHz ^{1}H TPPM decoupling (6.7 μs, 15°), 17.28 ms t_1 acquisition time (96×180 μs) with TPPI detection, 61.44 ms t_2 acquisition time (4096×15 μs), 2 s pulse delay. The data were processed with 65 Hz and 45 net line broadening (Lorentzian-to-Gaussian apodization) in ω_2 and ω_1 dimension separately and zero filled to 16384 (ω_2) × 384 (ω_1) complex points prior to Fourier transformation.

To test this approach experimentally, we acquired the first row of 2D ^{13}C–^{13}C experiments with varied r-SNOB pulse widths and found that r-SNOB pulse of an integer number of rotor periods gives only 77% of the signal obtained by applying an r-SNOB pulse of an integer plus half rotor periods. The percentage is the same as calculated from the initial signal intensity in the time domain extracted from the simulated rotational echoes illustrated in Fig. 6D. Complete 2D data sets were acquired for the two extreme cases, i.e., an integer and an integer plus half rotor periods. As shown in Fig. 8, significant dispersion components were observed for the diagonal peak when an r-SNOB pulse of 10 rotor periods were applied to C′ resonance of NAV. Therefore, the destructive interference

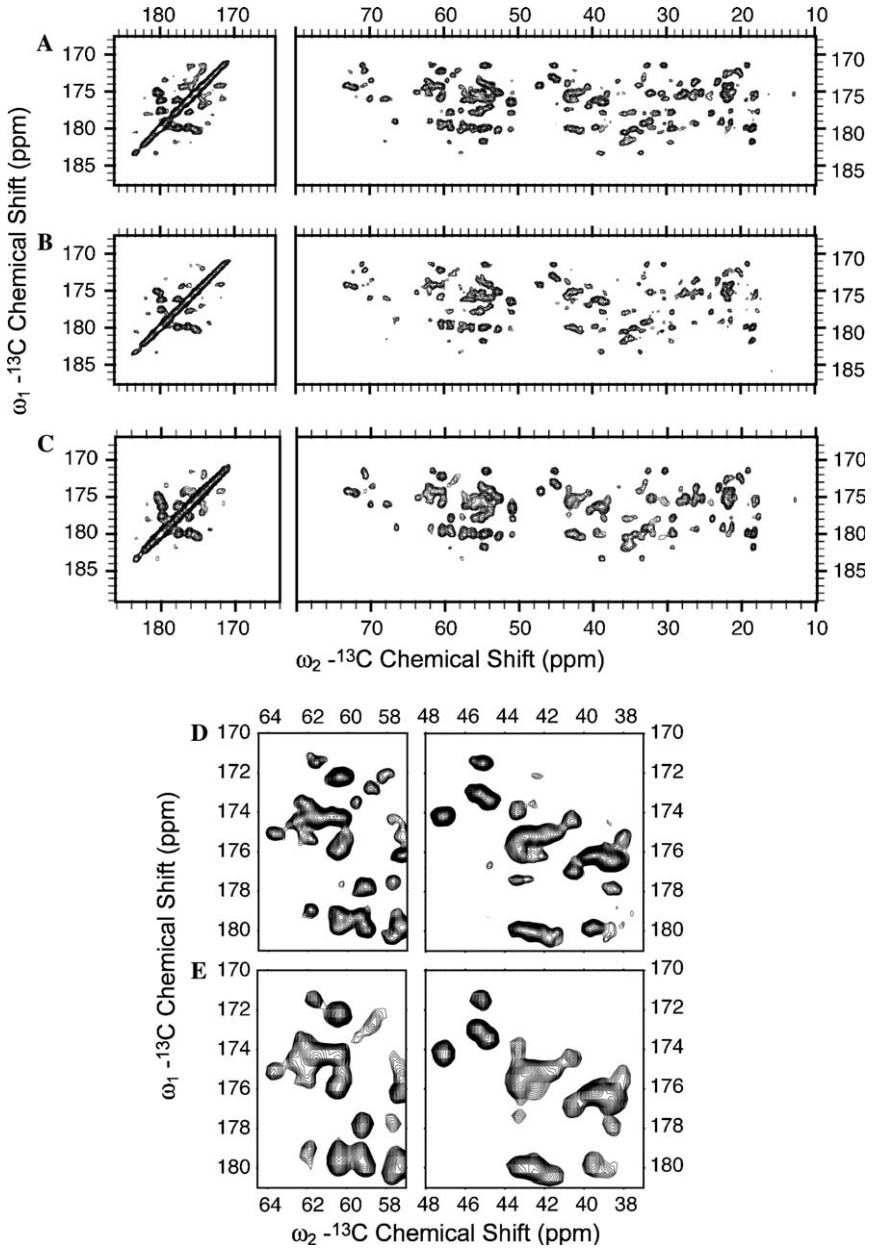

Fig. 9. 2D ^{13}C–^{13}C spectra of GB1 at 500 MHz ^{1}H frequency. (A) *J*-decoupled 2D ^{13}C–^{13}C spectrum with 750 μs r-SNOB on C′. (B) *J*-decoupled 2D ^{13}C–^{13}C spectrum with 800 μs r-SNOB on C′. (C) 2D^{13}C–^{13}C spectrum with no ^{13}C decoupling pulses. (D) Expansion of selected regions of *J*-decoupled 2D ^{13}C–^{13}C spectrum with 750 μs r-SNOB on C′. (E) Expansion of selected regions of 2D^{13}C–^{13}C spectrum with no decoupling pulses. The signal cutoff is 6σ noise level for (A), (B) and (D), 24σ noise level for (C) and (E). The rotor period is 100 μs. Other acquisition parameters are 1.5 ms ^{1}H–^{13}C CP contact time, 75 kHz ^{1}H TPPM decoupling (6.7 μs, 15°) during acquisition, 100 kHz ^{1}H TPMM decoupling (4.8 μs, 17°) during r-SNOB, 19.2 ms t_1 acquisition time (96 × 200 μs for *J*-decoupled spectra, 1536 × 12.5 μs for reference spectrum), 32.0 ms t_2 acquisition time (2560 × 12.5 μs) and 2 s pulse delay. All spectra were acquired with eight scans but signal cutoff of each spectrum is adjusted to reflect the difference in the number of points in the indirect dimension. The data were processed with 30 Hz net line broadening (Lorentzian-to-Gaussian apodization) for both dimensions and 70° shifted sine bell apodization in ω_1 dimension. The data were zero filled to 10,240 (ω_2) × 384 (ω_1) complex points for (A) and (B), 10,240 (ω_2) × 3072 (ω_1) complex points for (C) prior to Fourier transformation.

between the rotational echo and the hard π pulse not only causes signal loss but also leads to an undesirable line shape in multi-dimensional correlation spectra. For the Cα resonance, the difference is not as significant due to its smaller CSA magnitude. After establishing the correct rotor synchronization condition, we subsequently measured the signal retention from cross peak volumes. Compared to reference spectra without *J*-decoupling, the signal retention is 88% for C′ and 80% for Cα. The remaining difference is presumably due to the ^{1}H decoupling effects.

3.5. 2D ^{13}C–^{13}C correlation experiments with J-decoupling on GB1

In a typical multi-dimensional protein spectrum, the signal-to-noise ratio is much lower compared to that in amino acids or small peptides. Therefore, the ^{1}H decoupling and the rotor-synchronization problem discussed in previous sections are particularly important to detect and resolve weak signals. As an example to demonstrate the overall performance of computer-optimized selective pulses on a protein sample, we acquired 2D *J*-decoupled ^{13}C–^{13}C spectra on the β1 immunoglobulin binding domain of protein G (GB1) with an r-SNOB pulse applied to the C′ resonances. r-SNOB is chosen based on its higher time efficiency and less demanding decoupling requirement. Figs. 9A and B show the 2D ^{13}C–^{13}C spectra with 750 μs (7.5 rotor periods) and 800 μs (8 rotor periods) r-SNOB decoupling pulses applied separately. Fig. 9C shows the reference 2D spectrum without decoupling pulses. The refocusing efficiency of the 750 μs r-SNOB pulse is 95% in terms of the overall integrated C′ signals under 100 kHz ^{1}H TPPM decoupling during the r-SNOB pulse. Table 1 shows the comparison of line widths for some of the resolved cross-peaks in reference and *J*-decoupled spectra. Up to 57 Hz improvements in line width result in many more peaks resolved in the *J*-decoupled spectrum. The difference in signal intensity between Figs. 9A and B is significant especially in the region near the diagonal, where multiple additional peaks fall under the 6σ noise level in Fig. 9B due to the incorrect rotor synchronization condition. The overall decreased peak intensities are also observed in the aliphatic region and specifically the weak Ile6 C′–Cδ cross peak at (175.3, 12.8 ppm) is not present in Fig. 9B but in Fig. 9A. Figs. 9D and E show the expansion of two regions of *J*-decoupled and reference spectra, which illustrate the improved resolution in *J*-decoupled spectrum.

4. Conclusions

We have shown that r-SNOB and RE-BURP pulses give frequency profiles that are close to the originally designed target profiles for both Cα and C′ resonances of model peptide *N*-acetyl-Valine (NAV) under moderate MAS rates. Although the RF power must be adjusted to compensate for the crystallite orientation dependent RF scaling caused by CSA, large CSA magnitude is not the major source of magnetization loss during selective pulses if the spinning rate is sufficiently large compared to the magnitude of CSA. Instead, insufficient heteronuclear ^{1}H decoupling could be a major contribution to signal loss. TPPM ^{1}H decoupling was found to be more efficient than CW decoupling during the selective pulses, especially when the pulse duration is relatively long. Furthermore, signal loss and line shape perturbations in multi-dimensional experiments can be avoided by proper timing of selective pulses with respect to the rotor period. Selective pulses of an integer number of rotor periods cause a shift in the rotational echo by a half rotor period, so that selective pulses of an integer plus half rotor periods retain the maximal rotational echo intensity. This results in unperturbed line shapes in the indirect chemical shift dimensions of *J*-decoupling experiments and enables the use of rotor-synchronized sampling scheme as if no selective pulses were applied. Under optimal decoupling and correct rotor synchronization condi-

Table 1
Comparison of line widths in reference and *J*-decoupled 2D ^{13}C–^{13}C spectra

Cross-peak	Chemical shift in ω_1 dimension (ppm)	Line width[a] in reference spectrum (Hz)	Line width[a] in *J*-decoupled spectrum (Hz)	Difference in line width (Hz)
M1C′-CA	171.5	109	82	27
M1C′-CB	171.5	113	88	25
M1C′-CG	171.5	106	86	20
G14C′-CA	171.5	97	78	19
T16C′-CB	172.2	124	103	21
T18C′-CB	171.4	134	77	57
T18C′-CG	171.4	98	81	17
A20C′-CB	177.9	98	81	17
A24C′-CA	181.7	93	80	13
A24C′-CB	181.8	90	76	14
E27CD-CB	181.9	94	91	3
G38C′-CA	174.2	127	89	38
E56CD-CB	183.3	105	73	32
E56CD-CG	183.3	108	83	25

[a] The data were processed with 30 Hz net line broadening (Lorentzian-to-Gaussian apodization). Line widths were determined using Sparky (T.D. Goddard and D.G. Kneller, SPARKY 3, University of California, San Francisco).

tions, 2D ^{13}C–^{13}C spectra with *J*-decoupling acquired on a protein GB1 show improved resolution and high refocusing efficiency.

Acknowledgments

This research was supported by the University of Illinois (startup funds to C.M.R.), the Research Corporation (Research Innovation Award) and the National Science Foundation (CAREER Award, MCB 0347824). The authors thank Dr. Paul Molitor (VOICE NMR Facility, School of Chemical Sciences, University of Illinois) for technical assistance, and John Boettcher and Trent Franks for preparation of the GB1 sample.

References

[1] R. Freeman, Shaped radiofrequency pulses in high resolution NMR, Prog. NMR Spec. 32 (1998) 59–106.
[2] M. Gueron, P. Plateau, M. Decorps, Solvent signal suppression in NMR, Prog. NMR Spec. 23 (1991) 135–209.
[3] S.K. Straus, T. Bremi, R.R. Ernst, Experiments and strategies for the assignment of fully $^{13}C/^{15}N$-labelled polypeptides by solid state NMR, J. Biomol. NMR 12 (1998) 39–50.
[4] L. Duma, S. Hediger, A. Lesage, D. Sakellariou, L. Emsley, Carbon-13 lineshapes in solid-state NMR of labeled compounds. Effects of coherent CSA-dipolar cross-correlation, J. Magn. Reson. 162 (2003) 90–101.
[5] T.I. Igumenova, A.E. McDermott, Improvement of resolution in solid state NMR spectra with *J*-decoupling: an analysis of lineshape contributions in uniformly ^{13}C-enriched amino acids and proteins, J. Magn. Reson. 164 (2003) 270–285.
[6] S.K. Straus, T. Bremi, R.R. Ernst, Resolution enhancement by homonuclear *J* decoupling in solid-state MAS NMR, Chem. Phys. Lett. 262 (1996) 709–715.
[7] A. Bockmann, A. Lange, A. Galinier, S. Luca, N. Giraud, M. Juy, H. Heise, R. Montserret, F. Penin, M. Baldus, Solid state NMR sequential resonance assignments and conformational analysis of the 2×10.4 kDa dimeric form of the *Bacillus subtilis* protein Crh, J. Biomol. NMR 27 (2003) 323–339.
[8] T.I. Igumenova, A.E. McDermott, Homo-nuclear C-13 *J*-decoupling in uniformly C-13-enriched solid proteins, J. Magn. Reson. 175 (2005) 11–20.
[9] L. Duma, S. Hediger, A. Lesage, L. Emsley, Spin-state selection in solid-state NMR, J. Magn. Reson. 164 (2003) 187–195.
[10] L. Duma, S. Hediger, B. Brutscher, A. Bockmann, L. Emsley, Resolution enhancement in multidimensional solid-state NMR spectroscopy of proteins using spin-state selection, J. Am. Chem. Soc. 125 (2003) 11816–11817.
[11] C.P. Jaroniec, B.A. Tounge, C.M. Rienstra, J. Herzfeld, R.G. Griffin, Measurement of C-13–N-15 distances in uniformly C-13 labeled biomolecules: *J*-decoupled REDOR, J. Am. Chem. Soc. 121 (1999) 10237–10238.
[12] M. Hong, X.L. Yao, Homonuclear decoupled C-13 chemical shift anisotropy in C-13 doubly labeled peptides by selective-pulse solid-state NMR, J. Magn. Reson. 160 (2003) 114–119.
[13] B.J. Wylie, W.T. Franks, D.T. Graesser, C.M. Rienstra, Site-specific ^{13}C chemical shift anisotropy measurements in a uniformly ^{15}N, ^{13}C-labeled microcrystalline protein by 3D magic-angle spinning NMR spectrocopy, J. Am. Chem. Soc. 127 (2005) 11946–11947.
[14] C.P. Jaroniec, B.A. Tounge, J. Herzfeld, R.G. Griffin, Frequency selective heteronuclear dipolar recoupling in rotating solids: Accurate C-13–N-15 distance measurements in uniformly C-13,N-15-labeled peptides, J. Am. Chem. Soc. 123 (2001) 3507–3519.
[15] C.P. Jaroniec, J.C. Lansing, B.A. Tounge, M. Belenky, J. Herzfeld, R.G. Griffin, Measurement of dipolar couplings in a uniformly C-13,N-15-labeled membrane protein: distances between the Schiff base and aspartic acids in the active site of bacteriorhodopsin, J. Am. Chem. Soc. 123 (2001) 12929–12930.
[16] L. Kaustov, S. Kababya, V. Belakhov, T. Baasov, Y. Shoham, A. Schmidt, Inhibition mode of a bisubstrate inhibitor of KDO8P synthase: a frequency-selective REDOR solid-state and solution NMR characterization, J. Am. Chem. Soc. 125 (2003) 4662–4669.
[17] E. Kupce, G. Wagner, Multisite band-selective decoupling in proteins, J. Magn. Reson. B 110 (1996) 309–312.
[18] D. Nietlispach, A selective intra-HN(CA)CO experiment for the backbone assignment of deuterated proteins, J. Biomol. NMR 28 (2004) 131–136.
[19] H. Geen, R. Freeman, Band-selective radiofrequency pulses, J. Magn. Reson. 93 (1991) 93–141.
[20] E. Kupce, J. Boyd, I.D. Campbell, Short selective pulses for biochemical applications, J. Magn. Reson. B 106 (1995) 300–303.
[21] L. Emsley, G. Bodenhausen, Optimization of shaped selective pulses for NMR using a quaternion description of their overall propagators, J. Magn. Reson. 97 (1992) 135–148.
[22] L. Emsley, G. Bodenhausen, Gaussian pulse cascades—new analytical functions for rectangular selective inversion and in-phase excitation in NMR, Chem. Phys. Lett. 165 (1990) 469–476.
[23] P.J. Carroll, P.L. Stewart, S.J. Opella, Structures of two model peptides: *N*-acetyl-D,L-valine and *N*-acetyl-L-valyl-L-leucine, Acta Cryst. C 46 (1990) 243–246.
[24] W.T. Franks, D.H. Zhou, B.J. Wylie, B.G. Money, D.T. Graesser, H.L. Frericks, G. Sahota, C.M. Rienstra, Magic-angle spinning solid-state NMR spectroscopy of the beta1 immunoglobulin binding domain of protein G (GB1): ^{15}N and ^{13}C chemical shift assignments and conformational analysis, J. Am. Chem. Soc. 127 (2005) 12291–12305.
[25] A.E. Bennett, C.M. Rienstra, M. Auger, K.V. Lakshmi, R.G. Griffin, Heteronuclear decoupling in rotating solids, J. Phys. Chem. 103 (1995) 6951–6958.
[26] X.L. Wu, P. Xu, R. Freeman, A new kind of selective excitation sequence, J. Magn. Reson. 83 (1989) 404–410.
[27] K. Takegoshi, S. Nakamura, T. Terao, C-13–H-1 dipolar-assisted rotational resonance in magic-angle spinning NMR, Chem. Phys. Lett. 344 (2001) 631–637.
[28] M. Bak, J.T. Rasmussen, N.C. Nielsen, SIMPSON: a general simulation program for solid-state NMR spectroscopy, J. Magn. Reson. 147 (2000) 296–330.
[29] J.C.C. Chan, R. Tycko, Recoupling of chemical shift anisotropies in solid-state NMR under high-speed magic-angle spinning and in uniformly ^{13}C-labeled systems, J. Phys. Chem. 118 (2003) 8378–8389.
[30] M. Bak, N.C. Nielsen, REPULSION, A novel approach to efficient powder averaging in solid-state NMR, J. Magn. Reson. 125 (1997) 132–139.
[31] P. Borgnat, A. Lesage, S. Caldarelli, L. Emsley, Narrowband linear selective pulses for NMR, J. Magn. Reson. A 119 (1996) 289–294.
[32] D.P. Raleigh, M.H. Levitt, R.G. Griffin, Rotational resonance in solid state NMR, Chem. Phys. Lett. 146 (1988) 71–76.
[33] M. Veshtort, R.G. Griffin, High-performance selective excitation pulses for solid- and liquid-state NMR spectroscopy, Chem. Phys. Chem. 5 (2004) 834–850.
[34] P. Caravatti, G. Bodenhausen, R.R. Ernst, Selective pulse experiments in high-resolution solid state NMR, J. Magn. Reson. 55 (1983) 88–103.
[35] M.H. Levitt, Why do spinning sidebands have the same phase? J. Magn. Reson. 82 (1989) 427–433.